Article:
Han, Q., Li, M., Wang, Z. orcid.org/0000-0001-8142-1154 et al. (2 more authors) (2023) Local buckling behaviour and design of aluminium alloy plates in fire. Thin-Walled Structures, 189. 110886. ISSN 0263-8231

https://doi.org/10.1016/j.tws.2023.110886

Han QH, Li MY, Wang ZX, Yun X, Ouyang YW. Local buckling behaviour and design of aluminium alloy plates in fire. Thin-Walled Structures, 2023 (0263-8231).

Local buckling behaviour and design of aluminium alloy plates in fire

Qinghua Han[1,2,3], Mengyu Li[2], Zhongxing Wang[1,2,3], Xiang Yun[4], Yuanwen Ouyang[5,6]

[1]*Key Laboratory of Earthquake Engineering Simulation and Seismic Resilience of China, Earthquake Administration (Tianjin University), Tianjin 300350, China*
[2]*School of Civil Engineering, Tianjin University, Tianjin 300350, China*
[3]*Key Laboratory of Coast Civil Structure Safety of China Ministry of Education (Tianjin University), Tianjin 300350, China*
[4]*Department of Civil and Structural Engineering, University of Sheffield, Sheffield S1 3JD, UK*
[5]*Shanghai Tongzheng Aluminium Structure Construction & Technology Co., Ltd., Shanghai 201612, China*
[6]*Shanghai Jianke Aluminium Structure & Architecture Research Institute, Shanghai 201612, China*

Abstract

This paper presents a comprehensive study into the local buckling behaviour and design of aluminium alloy plates in fire. Finite element (FE) models were firstly developed to replicate the structural performance of aluminium alloy plates in fire obtained from fire tests collected from the existing literature. Upon validation of the FE models, comprehensive numerical parametric analyses were carried out considering a wide range of aluminium alloy grades, plate slendernesses, temperature levels as well as boundary and loading conditions. The obtained numerical results were then utilised to evaluate the accuracy of current design methods for aluminium alloy plates in fire. It has been found that the current design methods provide rather conservative and scattered resistance predictions for aluminium alloy plates in fire. To address the shortcomings of the existing design approaches, new cross-section classification limits and effective thickness method, taking due consideration of the variation in strength and stiffness of aluminium alloys at different elevated temperatures, were proposed. The new method is shown to be able to eliminate the discontinuity of the resistance predictions of aluminium alloy plates in fire in the European code and provide an improved level of buckling resistances, in terms of accuracy and consistency.

Keywords: Aluminium alloy; Cross-section behaviour; Effective thickness method; Fire; Local buckling; Plate; Slenderness limit.

1. Introduction

Aluminium alloys are becoming increasingly popular in structural applications, owing to their light weight, aesthetic appearance, ease of fabrication and good corrosion resistance. However, aluminium alloys are prone to fire damage due to notable deterioration of their mechanical properties at elevated temperatures [1], as indicated in Fig. 1 where the elevated temperature reduction factors for the Young's modulus and yield strength of aluminium alloys, carbon steels and stainless steels are compared. Moreover, aluminium alloy structural elements are prone to local buckling as a result of the relatively low value of the Young's modulus of the material (i.e. normally one third of that of the carbon steels) and the slender nature of the structural elements commonly used in practice [2,3]. Current fire design codes for aluminium alloy structures adopt the cross-section classifications and design formulae for local buckling specified in the room temperature standards, failing to accurately represent the local buckling behaviour of aluminium alloy structures in fire [4]. In order to prevent the premature collapse of aluminium alloy structures in fire, the development of a more reliable and rational local buckling design method for aluminium alloy structures at elevated temperatures is imperative.

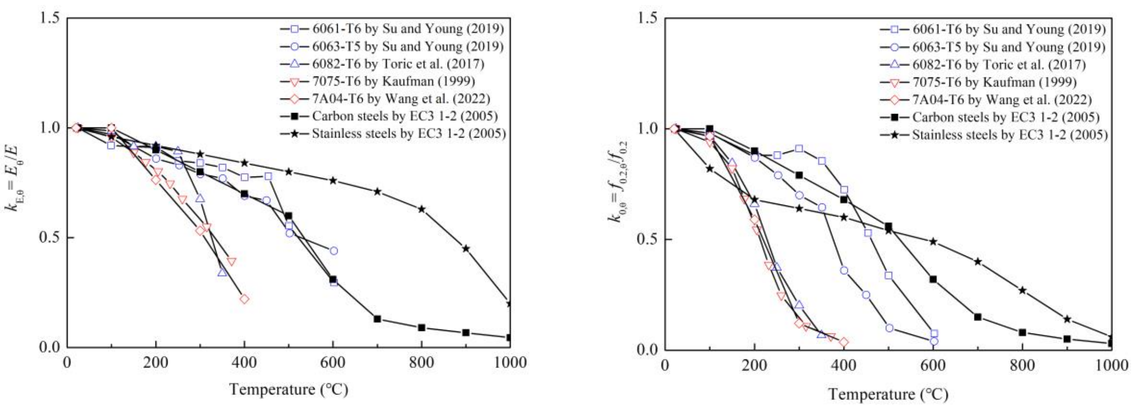

(a) Young's modulus (b) Yield strength

Fig. 1. Comparison of reduction factors for Young's modulus and yield strength of aluminium alloys, carbon steels and stainless steels at elevated temperatures [5-9]

In recent decades, extensive experimental and numerical studies have been performed on the local buckling behaviour of metallic (e.g. carbon steels, stainless steels and aluminium alloys) structural elements in fire. Among these studies, the investigation into the local buckling behaviour of plate elements is commonly deemed to be fundamental for the study of the local buckling behaviour of structural elements. Couto et al. [10] performed numerical studies on carbon steel plates in fire and introduced additional parameters into the design formulae for local buckling resistances in EN 1993-1-5 [11] to consider the influence of imperfections, steel grades and degrees of nonlinearity of the stress-strain relationships in fire. Similar investigations were conducted by Xing et al. [12] on the local buckling behaviour of stainless steel plates in fire, where modified equations, taking into account the varied deterioration rates of the mechanical properties of stainless steels at different elevated temperatures, were proposed. More recently, Kucukler [13] investigated the local buckling behaviour of both normal and high strength steel plates in fire and proposed a new design method with improved accuracy. With regards to the local buckling behaviour of cross-sections, Wang et al. [14,15] conducted stub column tests in fire covering a wide range of steel grades; the test results were used to evaluate the elevated-temperature design method for local buckling specified in EN 1993-1-2 [9]. The comparisons revealed that the EN 1993-1-2 [9] generally provides unconservative resistance predictions for stub columns in fire. The shortcomings of the fire design rules for local buckling provided in EN 1993-1-2 [9] were also highlighted by Yun et al. [16], in which a deformation based approach named the Continuous Strength Method was extended to the calculation of the fire resistances of hot-rolled steel tubular sections under combined loading, yielding more consistent resistance predictions than the design method given in EN 1993-1-2 [9]. Yang et al. [17] carried out a total of 24 stub column tests to investigate the local buckling performance of H- and box sections made of fire-resisting steel in fire; on the basis of the test results, the slenderness limit between the compact and non-compact sections specified in the American design code [18] was modified. Maljaars et al. [19-21] conducted tests on 6060-T66 and 5083-H111 aluminium alloy stub columns in fire and concluded that different deterioration rates of yield strength and stiffness of aluminium alloys in fire delayed the occurrence of local buckling of the stub columns. Maljaars et al. [19-21] also emphasised that attention should be paid to the influence of the more curved stress-strain relationships of aluminium alloys in fire on the local buckling behaviour of the structural elements. van der Meulen [22] carried out tests on 6060-T66 aluminium alloy beams in fire and proposed new slenderness limits for cross-section classifications and modified the design method for plates set out in EN 1999-1-2 [23]. It can be seen from the above literature review that far less investigations have been performed into the local buckling behaviour of aluminium alloy structures. Given that aluminium alloys display distinct mechanical properties in fire, such as more curved stress-strain relationships and varying deterioration rates of yield strength and elastic modulus, it is crucial to conduct a comprehensive study on the local buckling behaviour of these alloys to gain a better understanding of their performance in high-temperature scenarios.

The present study is carried out with the aim of elucidating the mechanism of local buckling of aluminium alloy plates in high-temperature environments and proposing an accurate design methodology based on a comprehensive analysis of numerically-obtained structural performance data. Firstly, a comprehensive numerical study into the local buckling behaviour of aluminium alloy plates in fire is presented in this paper. Finite element (FE) models were first developed to replicate the structural performance of aluminium alloy plates in fire and validated against fire test results collected from the literature. Following this, extensive parametric studies, covering a wide range of temperature levels, plate slendernesses, aluminium alloy grades as well as boundary and loading conditions, were preformed utilising the validated numerical models. The accuracy of the existing design methods for the local buckling assessment of aluminium alloy plates in fire, including the current codified design provisions in European (EN 1999-1-2) [23], Chinese (T/CECS 756-2020) [24] and American (AA 2015) [25] specifications as well as the Continuous Strength Method (CSM) [26] and recent proposals by Maljaars et al. [21] and van der Meulen [22], were evaluated through comparisons with the data obtained from the numerical parametric studies. Shortcomings of the existing design methods for the local buckling design of aluminium alloy plates in fire were identified. With the aim to improve the accuracy of the design approach, new cross-section classifications and design methods for the determination of load-carrying capacities of aluminium alloy plates in fire were proposed underpinned by a significant amount of data points generated in the current paper and collected from the literature. Finally, the reliability of the new proposal and the existing design methods were carefully assessed in accordance with three safety criteria proposed by Kruppa [27] for structural fire design.

2. Finite element (FE) analysis

2.1 Modelling assumptions

The FE models in the present paper were developed using the finite element software package ABAQUS [28]. Measured stress-strain curves of aluminium alloys at elevated temperatures collected from the literature were adopted in the numerical analyses for validation purposes. It should be noted that the measured engineering stress-strain curves were converted into the true stress-logarithmic plastic true strain curves before being incorporated into ABAQUS. The four-noded general purpose shell element with reduced integration, referred to as S4R in ABAQUS [28], being capable of considering membrane strains and transverse shear deformations, was employed in the present study. This element type has been successfully used to mimic the local buckling behaviour of similar structural elements at both ambient [29] and elevated [30] temperatures. A mesh size equal to 1/20 of the plate width (b) was adopted for the FE models following a thorough mesh sensitivity analysis; this mesh size was fine enough to yield a high level of computational accuracy with reasonable computational times.

The simply supported (SS) boundary condition was adopted for plate models, as shown in Fig. 2, where b and l represent the width and length of the plate. For the internal plate (i.e. SS on four edges), translations in Z direction of all four edges and in Y direction of the two transversal edges were restrained, while other translational degrees of freedom (DOFs) and all rotational DOFs were released, as shown in Fig. 2 (a). For the outstand plate (i.e. SS on three edges), the boundary conditions were identical to those of the internal plate except for a totally free longitudinal edge, as shown in Fig. 2 (b). Two reference points (RP1 and RP2), as shown in Fig. 2, were constrained to the nodes at the corresponding transversal edge and different loading conditions were applied to the reference points through displacement-controlled procedure.

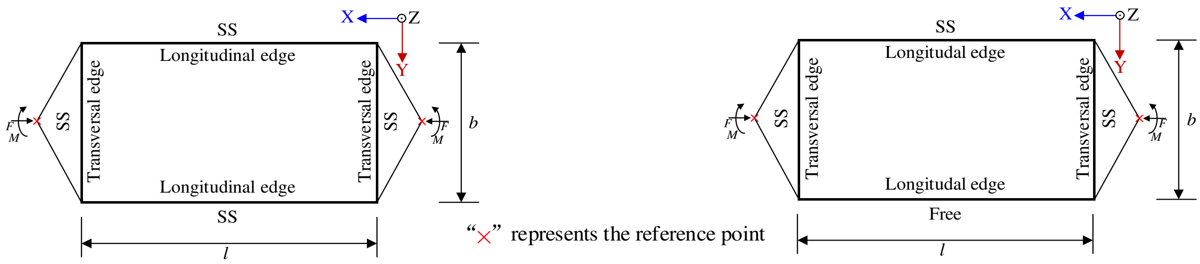

(a) Internal plate (b) Outstand plate

Fig. 2. Boundary conditions of internal and outstand plates

Initial local geometric imperfections, assumed to be in the form of the lowest elastic local buckling mode shape under compression, were also incorporated into the FE models. The measured local imperfection amplitudes w_L of aluminium alloy internal and outstand plates [2,31,32-36] are summarised in Table 1 and Fig. 3, where the average measured local imperfection amplitudes for these plates are also provided in Table 1. As shown in Table 1, the average values of measured imperfection amplitudes for the collected internal and outstand aluminium alloy plates are b/1000 and b/250, respectively, which are considerably lower than the fabrication tolerance-based local geometric imperfection amplitudes (i.e. b/200 and b/100 for internal and outstand plates, respectively, as specified in EN 1090-2 [37] and EN 1090-3 [38]). The influence of residual stress on the buckling resistances of aluminium alloy plates was found to be negligible [1] and thus not involved in the developed FE models.

Table 1 Summary of measured local imperfection amplitudes of aluminium alloy internal and outstand plates

Reference	Plate type	Number of collected data	Average
Wang et al. [2]	Internal plate	4	$b/667$
Maljaars et al. [20]	Internal plate	27	$b/1000$
van der Meulen [22]	Internal plate	116	$b/1000$
Yuan et al. [31]	Internal plate	15	$b/667$
Zhu et al. [32]	Internal plate	5	$b/333$
Wang et al. [33]	Internal plate	11	$b/667$
Feng et al. [34]	Internal plate	6	$b/400$
Zhu et al. [35]	Internal plate	3	$b/286$
All internal plates		187	$b/1000$
Wang et al. [2]	Outstand plate	4	$b/333$
Maljaars et al. [20]	Outstand plate	4	$b/333$
Yuan et al. [31]	Outstand plate	15	$b/333$
Wang et al. [33]	Outstand plate	11	$b/333$
Zhang et al. [36]	Outstand plate	8	$b/143$
All outstand plates		42	$b/250$

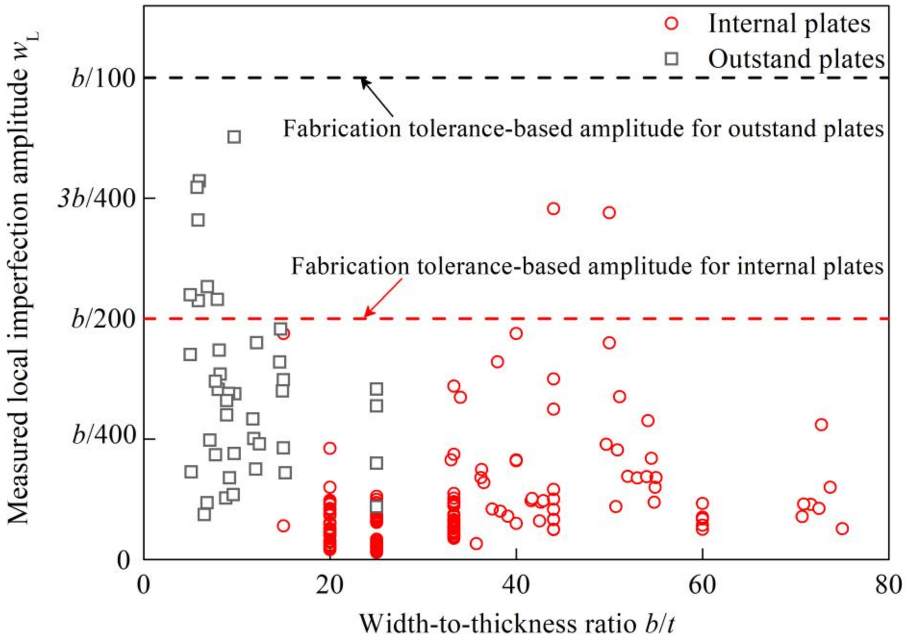

Fig. 3. Summary of measured local imperfection amplitudes of 187 internal and 42 outstand aluminium alloy plates

2.2 Validation

Test results of aluminium alloy structural elements subjected to compression and bending at elevated temperatures are collected and employed to validate the developed FE models.

2.2.1 Collected column and beam test results

Maljaars et al. [19] performed steady-state tests on 6060-T66 aluminium alloy stub columns made of square hollow sections (SHS) and equal angle sections to study the local buckling behaviour of aluminium alloy elements in fire, among which 17 specimens were fabricated from extrusion processes and were collected to validate the established FE models for plates in compression at elevated temperatures. The column length was equal to six times the cross-section width and the test temperatures ranged from room temperature to approximate 400 °C. van der Meulen [22] performed 12 steady-state three-point bending tests on 6060-T66 aluminium alloy beams made of SHS subjected to uniform temperatures ranging from 20 to 300 °C, the results of which were utilised to validate the FE models for plates in bending at elevated temperatures.

2.2.2 Validation of FE models for aluminium alloy plates in compression

The SHS and equal angle sections are composed of plates with identical plate slenderness, thus the interaction between adjacent plate elements is sufficiently small that can be neglected. In this section, the fire test results of SHS and equal angle sections in compression were utilised to assess the accuracy of the FE models for aluminium alloy plates in compression; note that the plate width and thickness of the FE model were taken as the average width and thickness of the constituent plates of the corresponding tested cross sections, respectively. The ultimate resistance of the plate FE model ($N_{u,FE}$) was multiplied by 4 and 2 for internal and outstand plates, respectively, before comparing with experimental results on cross sections ($N_{u,test}$). The comparison results are summarised in Tables 2 and 3 for internal and outstand plates in compression at elevated temperatures, respectively. The specimens in Tables 2 and 3 were labelled such that key parameters in experiments, such as the aluminium alloy grades, plate width-to-thickness ratios, boundary conditions (internal plate (I) or outstand plate (O)) and exposure temperatures can be clearly identified. For example, specimen T66-25-I-20 represents an internal 6060-T66 aluminium alloy plate, with a width-to-thickness ratio (b/t) of 25 at a test temperature of 20 °C. It should be noted that the last letter "r" in the labelling system indicates a repeat test. A sensitivity analysis was performed to investigate the sensitivity of the FE models to variations in the local imperfection amplitudes. A total of five different local imperfection amplitudes were considered, including the measured local imperfection amplitude and four generalised values of $b/100$, $b/200$, $b/300$ and $b/400$. It can be seen from Tables 2 and 3 that the local buckling resistances of aluminium alloy plates in pure compression, especially for internal plates with simply supported boundary conditions along the edges, are somewhat sensitive to the local imperfection amplitudes. The tolerance-based local geometric imperfection amplitudes (i.e. $b/200$ and $b/100$ for internal and outstand plates, respectively, as specified in EN 1090-2 [37] and EN 1090-3 [38]) were employed throughout the parametric study, enabling the generation of safe-sided numerical results.

It is worth noting that the significant differences observed between the experimental and numerical results for certain specimens may be attributed to the greater uncertainties inherent in structural fire tests, relative to room temperature tests, as well as the sensitivity of the material properties to loading rate, variations in temperature within the furnace, and deviations from the intended loading eccentricities. The comparisons of load-displacement curves and failure modes obtained from both finite element models and tests, as presented in Figs. 4 (a) and 5 (a) respectively, generally demonstrate a high degree of consistency. Thus, the numerical models developed in the present study were deemed capable of accurately predicting the structural behaviour of aluminium alloy plates under compression at elevated temperatures.

Table 2 Comparisons of FE and test results with different local imperfection amplitudes for aluminium alloy internal plates in compression under varying temperatures

Specimen label	$N_{u,test}$ (kN)	$N_{u,FE}/N_{u,test}$				
		Local imperfection amplitude				
		Measured	$b/100$	$b/200$	$b/300$	$b/400$
T66-25-I-20	78.80	1.05	0.90	0.96	0.99	1.00
T66-25-I-20r	79.10	1.04	0.89	0.95	0.97	1.00
T66-25-I-20r	81.00	1.05	0.93	0.98	1.01	1.02
T66-25-I-179	65.80	0.98	0.89	0.94	0.95	0.97
T66-25-I-265	28.80	1.01	0.93	0.98	1.00	1.00
T66-25-I-290	22.70	0.98	0.95	0.97	0.98	0.98
T66-44-I-20	26.80	1.10	1.02	1.08	1.10	1.11
T66-44-I-179	23.40	1.08	0.91	0.97	1.00	1.02
T66-44-I-268	13.10	0.83	0.81	0.85	0.93	0.96
T66-44-I-289	10.70	1.11	0.95	1.04	1.08	1.09
T66-44-I-287	11.90	1.00	0.83	0.93	0.95	0.98
T66-60-I-20	12.00	1.20	1.15	1.18	1.19	1.19
T66-60-I-20r	11.40	1.22	1.16	1.19	1.20	1.20
Mean		1.05	0.95	1.00	1.03	1.04
COV		0.100	0.112	0.097	0.086	0.078

Table 3 Comparisons of FE and test results with different local imperfection amplitudes for aluminium alloy outstand plates in compression under varying temperatures

Specimen label	$N_{u,test}$ (kN)	$N_{u,FE}/N_{u,test}$				
		Local imperfection amplitude				
		Measured	$b/100$	$b/200$	$b/300$	$b/400$
T66-25-O-20	19.90	1.23	1.23	1.23	1.23	1.23
T66-25-O-171	16.80	1.14	1.14	1.14	1.14	1.14
T66-25-O-267	8.44	1.09	1.06	1.07	1.08	1.08
T66-25-O-299	7.10	1.16	1.08	1.13	1.15	1.16
Mean		1.16	1.13	1.14	1.15	1.15
COV		0.050	0.068	0.058	0.054	0.054

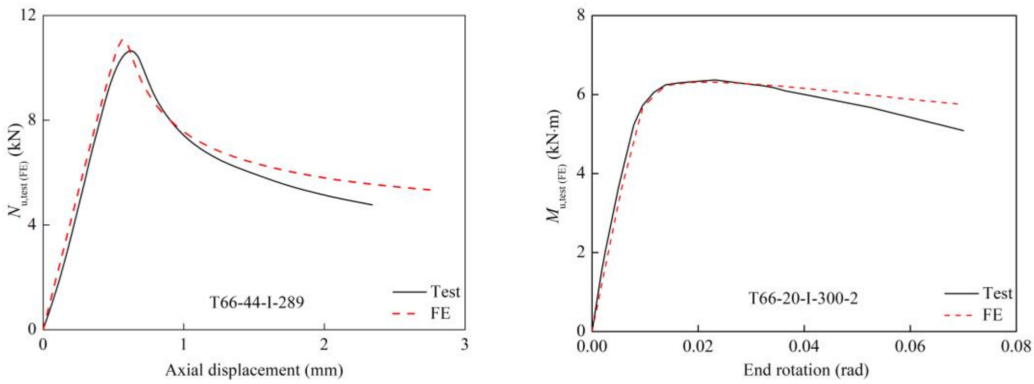

(a) Plates in compression (b) Plates in bending

Fig. 4. Comparisons of typical FE and test load-displacement (moment-rotation) curves for aluminium alloy plates at elevated temperatures

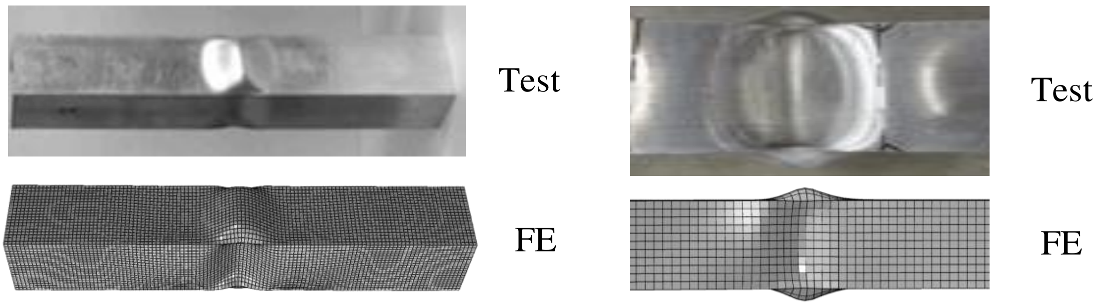

(a) Plates in compression (b) Plates in bending

Fig. 5. Comparisons of typical FE and test failure modes for aluminium alloy plates at elevated temperatures

2.2.3 Validation of FE models for aluminium alloy plates in bending

Since the determination of boundary conditions for individual plates in beams is rather complicated due to the existence of rotational restraint between adjoined plates, FE models of the entire beam were developed herein for the validation of aluminium alloy plates in bending; note that Xing et al. [12] adopted the similar validation approach for stainless steel plates in bending. The ultimate bending moments obtained from FE models ($M_{u,FE}$) and tests ($M_{u,test}$) are compared in Table 4. Note that the specimens in Table 4 adopt the same labelling system as that defined in Section 2.2.2, except for the last number which identifies the beam length (in metres). A similar sensitivity analysis on imperfection amplitudes was also carried out and the results are summarised in Table 4, indicating that plates in bending are generally less sensitive to imperfection amplitudes than that of plates in compression. Typical moment-rotation curves and failure modes obtained from numerical models and tests are compared in Figs. 4 (b) and 5 (b), respectively. It can be concluded from above comparison results that the developed numerical models can simulate the structural performance of aluminium alloy plates in bending at elevated temperatures accurately.

Table 4 Comparisons of FE and test results with different local imperfection amplitudes for aluminium alloy plates in bending under varying temperatures

Specimen label	$M_{u,test}$ (kN·m)	$M_{u,FE}/M_{u,test}$				
		Local imperfection amplitude				
		Measured	$b/100$	$b/200$	$b/300$	$b/400$
T66-33-I-20-2	17.70	1.05	1.03	1.04	1.04	1.05
T66-33-I-20-2r	17.59	1.05	1.02	1.03	1.04	1.04
T66-33-I-250-2	8.45	1.05	0.99	1.01	1.03	1.03
T66-33-I-300-2	3.82	1.02	0.99	1.01	1.02	1.02
T66-25-I-20-2	22.14	1.05	1.00	1.02	1.03	1.03
T66-25-I-250-1	8.42	1.08	1.07	1.07	1.08	1.08
T66-25-I-250-2	9.93	1.02	0.99	1.01	1.01	1.01
T66-25-I-300-2	5.18	1.04	1.02	1.03	1.03	1.04
T66-20-I-20-2	27.73	0.99	0.96	0.98	0.99	0.99
T66-20-I-250-1	10.77	1.00	0.99	1.00	1.00	1.00
T66-20-I-250-2	11.51	1.04	1.02	1.03	1.04	1.04
T66-20-I-300-2	6.53	0.97	0.96	0.97	0.97	0.97
Mean		1.03	1.00	1.02	1.02	1.02
COV		0.030	0.029	0.028	0.028	0.028

2.3 Parametric studies

Upon validation of the FE models, comprehensive parametric studies were carried out, covering a wide range of aluminium alloy grades, plate slendernesses, temperature levels as well as boundary and loading conditions, to generate sufficient structural fire performance data on aluminium alloy plates subjected to pure compression or pure bending. Three commonly used structural aluminium alloys: 6061-T6, 6063-T5 and 7A04-T6 [39], covering two buckling classes according to EN 1999-1-2 [23] (i.e. Class A and Class B) and both normal strength (i.e. 6000 series) and high strength (i.e. 7000 series) aluminium alloys, were adopted in the parametric studies. Key mechanical properties of the three different aluminium alloys at elevated temperatures as reported in [5,6] are summarised in Table 5, where E_θ is Young's modulus at temperature θ, $f_{0.2,\theta}$ and $f_{u,\theta}$ represent yield and ultimate strengths at temperature θ, respectively. The plate slenderness at temperature θ ($\bar{\lambda}_{p,\theta}$), defined as the square root of the ratio of $f_{0.2,\theta}$ to the elastic critical buckling stress at temperature θ ($\sigma_{cr,\theta}$), was selected to range between 0.2 to 2.0 with 0.1 intervals. The different plate slenderness values were achieved by varying the plate thickness while maintaining constant values for both the plate length and width. The plate length and width (l×b) were taken as 1600 mm×400 mm and 4000 mm×400 mm for internal and outstand plates, respectively. These dimensions were selected in order to avoid the length effects and ensure the critical buckling stresses obtained from the FE models being close to those determined from theoretical equations [40,41]; this is consistent with the previous investigations [12,13]. Seven temperature levels, including room temperature (20 °C), 100 °C, 200 °C, 300 °C, 400 °C, 500 °C and 600 °C, were analysed for 6000 series aluminium alloys; 7A04-T6 aluminium alloy almost loses strength and stiffness at 400 °C [5], hence higher temperature levels were not covered. Different boundary and loading conditions, including internal plates subjected to pure compression and pure bending and outstand plates subjected to compression, were investigated in the parametric studies. A total of 1995 FE models were generated, including 1330 plates in compression and 665 plates in bending. The obtained structural performance data were then applied to assess the accuracy of current design rules and underpin the development of a new design method as described in Section 4.

Table 5 Material properties of investigated aluminium alloys at elevated temperatures

Temperature (°C)	6061-T6			6063-T5			7A04-T6		
	E_θ (MPa)	$f_{0.2,\theta}$ (MPa)	$f_{u,\theta}$ (MPa)	E_θ (MPa)	$f_{0.2,\theta}$ (MPa)	$f_{u,\theta}$ (MPa)	E_θ (MPa)	$f_{0.2,\theta}$ (MPa)	$f_{u,\theta}$ (MPa)
20	69500	199.9	232.3	65600	186.6	226.8	68700	503.4	585.1
100	64000	195.2	225.1	63400	183.7	217.6	68700	486.4	527.4
200	63400	176.9	197.8	56100	163.1	183.4	50700	296.9	298.5
300	58500	181.0	189.1	51700	131.2	138.5	35300	61.1	64.7
400	52100	139.0	145.9	45300	67.9	71.0	14700	18.4	20.9
500	43100	80.7	85.1	34100	18.6	19.1	-	-	-
600	15700	17.5	20.6	28900	7.3	7.6	-	-	-

3. Assessment of existing design methods for aluminium alloy plates in fire

Different design methods for aluminium alloy plates in fire, including codified approaches specified in European (EN 1999-1-2 [23]), Chinese (T/CECS 756-2020 [24]) and American (AA 2015 [25]) standards, the Continuous Strength Method (CSM) [26] as well as recent proposals by Maljaars et al. [21] and van der Meulen [22], are first briefly introduced in this section. Then, FE results and resistance predictions obtained by these design approaches are compared and discussed. The quantitative assessment of all design methods is summarised in Table 7, where $N_{fi,pred,Rd}$ and $M_{fi,pred,Rd}$ represent predicted ultimate compressive and bending resistances, respectively. Note that in order to facilitate the direct comparison among different design methods, all partial safety factors are set equal to unity.

3.1 European (EN 1999-1-2) and Chinese (T/CECS 756-2020) codes

According to the design procedure specified in EN 1999-1-2 [23], the cross-section classification of an aluminium alloy plate at elevated temperatures should be first determined following the rules in the room temperature code, i.e. EN 1999-1-1 [42]. Following this, the design resistance of the plate is calculated as the product of the room temperature local buckling resistance determined by EN 1999-1-1 [42] and the reduction factor of yield strength at elevated temperature θ ($k_{0,\theta}$). The design resistances for different classes of plates are summarised in Table 6, in which $N_{\mathrm{fi,EN,Rd}}$ and $M_{\mathrm{fi,EN,Rd}}$ represent the compressive and bending resistances of a plate in fire predicted by EN 1999-1-2 [23], respectively, A and A_{eff} are respectively the gross and effective area of the cross section, and W_{pl}, W_{el} and W_{eff} are plastic, elastic and effective modulus of the cross section, respectively.

Table 6 Summary of cross-section classifications and design resistances for aluminium alloy plates in fire specified in EN 1999-1-2 [23] and T/CECS 756-2020 [24]

Cross-section classification in EN 1999-1-2	Cross-section classification in T/CECS 756-2020	Design compressive resistance ($N_{\mathrm{fi,EN/CECS,Rd}}$)	Design bending resistance ($M_{\mathrm{fi,EN/CECS,Rd}}$)
Class 1-2	Non-slender	$Af_{0.2}k_{0,\theta}$	$W_{\mathrm{pl}}f_{0.2}k_{0,\theta}$ ($W_{\mathrm{el}}f_{0.2}k_{0,\theta}$*)
Class 3		$Af_{0.2}k_{0,\theta}$	$W_{\mathrm{el}}f_{0.2}k_{0,\theta}$
Class 4	Slender	$A_{\mathrm{eff}}f_{0.2}k_{0,\theta}$	$W_{\mathrm{eff}}f_{0.2}k_{0,\theta}$

Note: *the spread of plasticity is not accounted for in Chinese code for the design of plates in bending

The unfavourable effects of local buckling for Class 4 plates are quantified by the effective cross-section area and modulus, i.e. A_{eff} and W_{eff}, which are determined by means of the effective thickness method. This method translates the non-uniform stress distribution along plate thickness (t) into a uniform stress distribution of $f_{0.2}$ in partial (or effective) thickness of the plate (t_{eff}), as expressed by Eq. (1),

$$t_{\mathrm{eff}} = \rho_{\mathrm{c,EN}}\, t \tag{1}$$

where $\rho_{\mathrm{c,EN}}$ is the effective thickness ratio in the European code [23], calculated following Eq. (2) in accordance with EN 1999-1-1 [42],

$$\rho_{\mathrm{c,EN}} = \frac{C_{1,\mathrm{EN}}}{\left(\beta_{\mathrm{EN}}/\varepsilon\right)} - \frac{C_{2,\mathrm{EN}}}{\left(\beta_{\mathrm{EN}}/\varepsilon\right)^2} \le 1 \tag{2}$$

in which $C_{1,\mathrm{EN}}$ and $C_{2,\mathrm{EN}}$ are constants related to buckling Class (i.e. A or B) of materials specified in EN 1999-1-1 [42] and boundary conditions (i.e. internal or outstand), β_{EN} is the slenderness ratio related to b/t and loading conditions, and $\varepsilon = (250/f_{0.2})^{1/2}$. Note that the room temperature material properties are used in Eq. (2) to determine the effective thickness ratio $\rho_{\mathrm{c,EN}}$ rather than the elevated-temperature material properties.

The Chinese code for the design of aluminium alloy structures in fire (T/CECS 756-2020) [24] generally follows the design procedures and methods specified in EN 1999-1-2 [23] for calculating the local buckling resistances of aluminium alloy plates, as summarised in Table 6. However, the Chinese code adopts only two cross-section classifications, named non-slender and slender, and utilises a different equation for the determination of the effective thickness ratio ρ_c, as given by Eq. (3),

$$\rho_{c,CECS} = C_{1,CECS}\frac{1}{\overline{\lambda}_p} - C_{2,CECS}\frac{0.22}{\overline{\lambda}_p^{\,2}} \leq 1 \tag{3}$$

where $\overline{\lambda}_p$ is the plate slenderness equal to the square root of the ratio of yield stress at room temperature $f_{0.2}$ to the elastic critical buckling stress σ_{cr}, and $C_{1,CECS}$ and $C_{2,CECS}$ are parameters that equivalent to $C_{1,EN}$ and $C_{2,EN}$ respectively in EN 1999-1-2 [23].

The ultimate compressive and bending resistances of aluminium alloy plates in fire obtained from numerical models and predicted according to EN 1999-1-2 [23] are normalised by $Af_{0.2,\theta}$ and $W_{pl}f_{0.2,\theta}$, respectively, and are plotted against the plate slenderness $\overline{\lambda}_p$, as shown in Figs. 6-8. As can be seen from the figures, the EN 1999-1-2 [23] generally provides inaccurate and rather conservative ultimate resistance predictions for aluminium alloy plates in fire, while the EN 1999-1-2 predictions lie on the unsafe side for 6061-T6 internal plates in compression at temperatures lower than 400 °C. For slender aluminium alloy plates, the EN 1999-1-2 [23] leads to an increasing conservatism of the resistance predictions with increasing temperatures; this may be attributed to the neglect of the different deterioration rates of stiffness (E_θ) and yield strength ($f_{0.2,\theta}$) of aluminium alloys in fire. With regards to stocky aluminium alloy plates, the EN 1999-1-2 [23] disregards the strain-hardening characteristic of aluminium alloys, resulting in rather conservative resistance predictions. The results summarised in Table 7 manifest that the resistance predictions according to EN 1999-1-2 [23] underestimate the resistances of aluminium alloy plates at 600 °C by approximate 50%, indicating the conservative nature of the code at high temperatures.

Comparisons between FE results and resistance predictions by T/CECS 756-2020 [24] are shown in Figs. 9-11 for internal aluminium alloy plates in pure compression and pure bending and outstand aluminium alloy plates in compression, respectively. As can be seen from these figures, the relationship between the degree of conservatism of T/CECS 756-2020 [24] and temperature levels is similar to that of EN 1999-1-2 [23]. As indicated by the results given in Table 7, the Chinese code generally provides more conservative and scattered resistance predictions than the European code for aluminium alloy plates in fire.

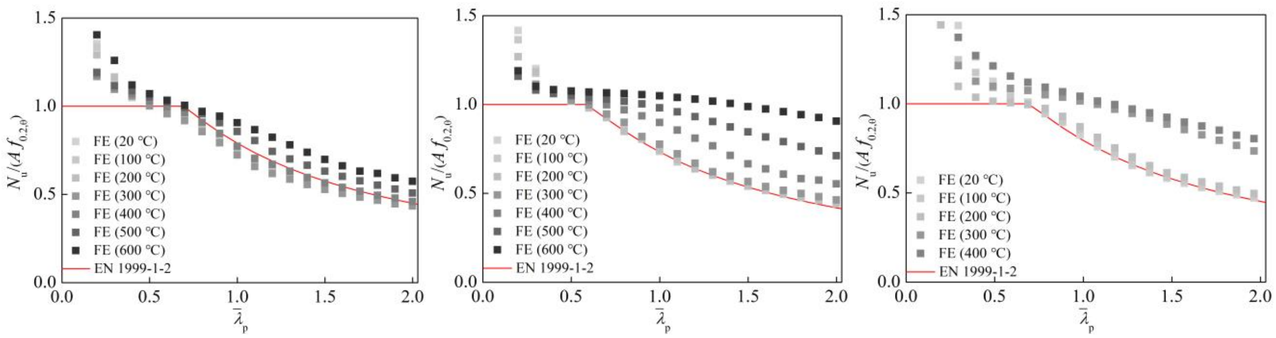

(a) 6061-T6 (b) 6063-T5 (c) 7A04-T6

Fig. 6. Comparisons between FE results and resistance predictions according to EN 1999-1-2 [23] for internal plates in compression at different elevated temperatures

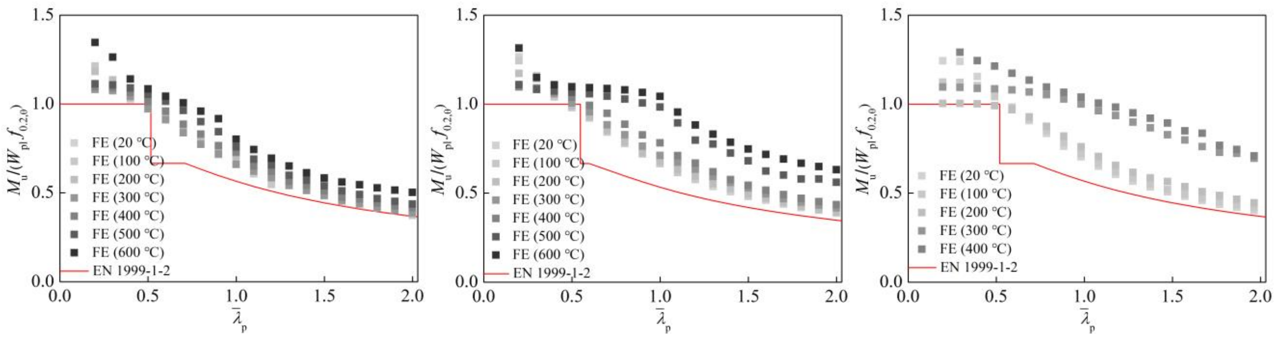

(a) 6061-T6 (b) 6063-T5 (c) 7A04-T6

Fig. 7. Comparisons between FE results and resistance predictions according to EN 1999-1-2 [23] for internal plates in bending at different elevated temperatures

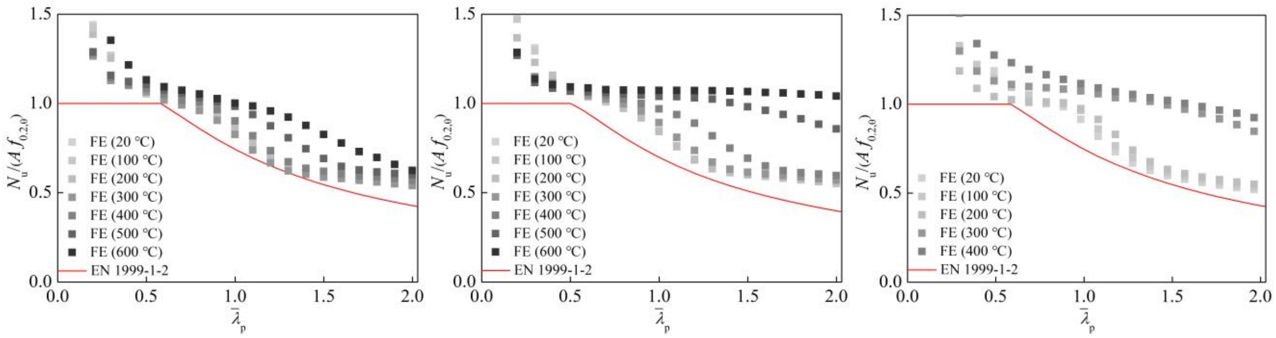

(a) 6061-T6 (b) 6063-T5 (c) 7A04-T6

Fig. 8. Comparisons between FE results and resistance predictions according to EN 1999-1-2 [23] for outstand plates in compression at different elevated temperatures

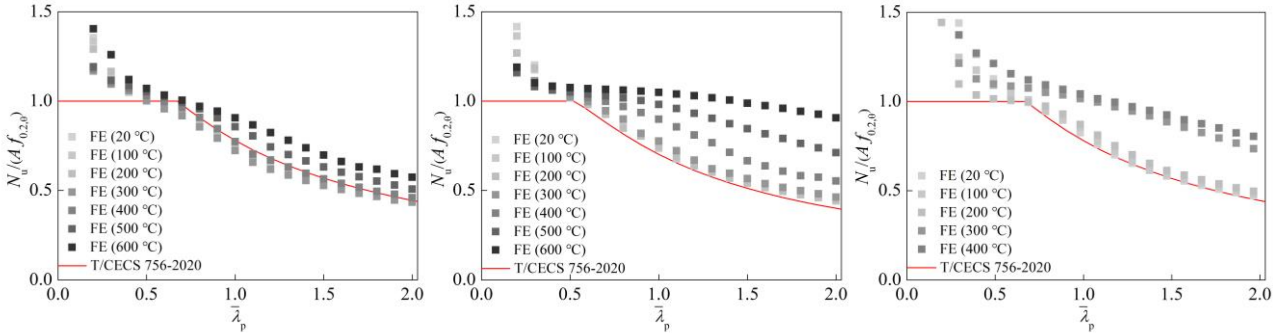

(a) 6061-T6 (b) 6063-T5 (c) 7A04-T6

Fig. 9. Comparisons between FE results and resistance predictions according to T/CECS 756-2020 [24] for internal plates in compression at different elevated temperatures

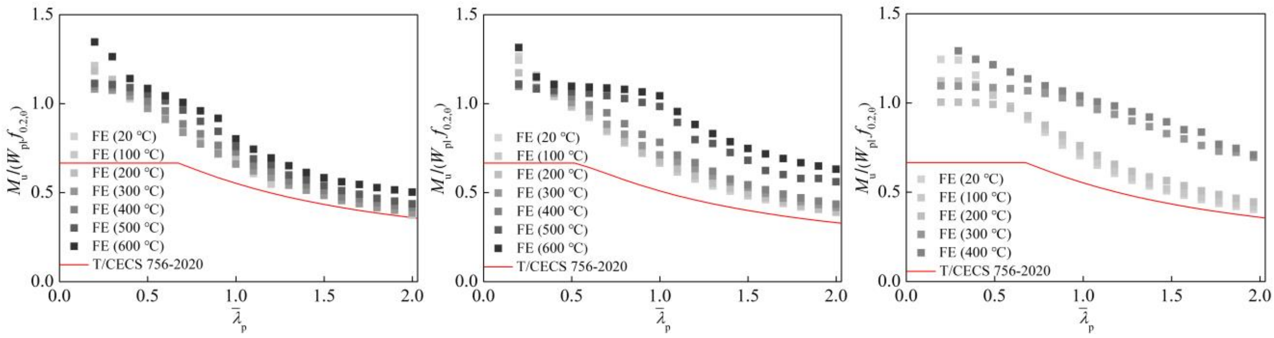

(a) 6061-T6 (b) 6063-T5 (c) 7A04-T6

Fig. 10. Comparisons between FE results and resistance predictions according to T/CECS 756-2020 [24] for internal plates in bending at different elevated temperatures

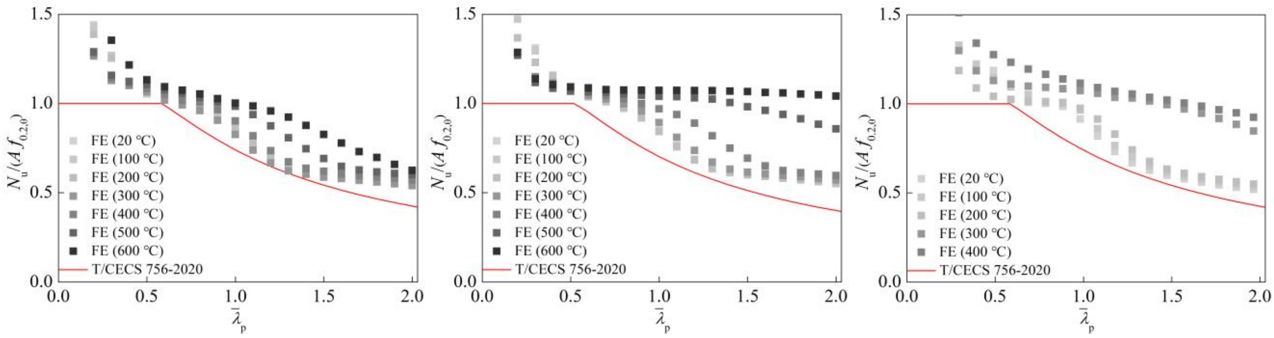

(a) 6061-T6 (b) 6063-T5 (c) 7A04-T6

Fig. 11. Comparisons between FE results and resistance predictions according to T/CECS 756-2020 [24] for outstand plates in compression at different elevated temperatures

3.2 American code (AA 2015)

The design methods for the local buckling resistances of aluminium alloy plates in fire specified in AA 2015 [25] adopt the same design formulae for aluminium alloy plates at the room temperature, while the elevated-temperature material properties are used instead, as given by Eqs. (4) and (5),

$$N_{\mathrm{fi,AA,Rd}} = F_{\mathrm{c},\theta} A \quad (4)$$

$$M_{\mathrm{fi,AA,Rd}} = F_{\mathrm{b},\theta} I_{\mathrm{w}} / c_{\mathrm{cw}} \quad (5)$$

where $F_{c,\theta}$ and $F_{b,\theta}$ are the uniform compressive strength and the flexural compressive strength of the aluminium alloy plate at temperature θ, respectively, which can be determined by using the formulae given in Sections B5.4 and B5.5 of AA 2015 [25], A and I_w are the area and the moment of inertia of the aluminium alloy plate, respectively, c_{cw} is the distance between the extreme compression fibre of the flexural compression part of the aluminium alloy plate to its neutral axis.

The resistance predictions according to AA 2015 [25] ($N_{fi,AA,Rd}$ and $M_{fi,AA,Rd}$) are compared with the numerically obtained results ($N_{u,FE}$ and $M_{u,FE}$), as shown in Figs. 12-14 for internal aluminium alloy plates in pure compression and pure bending and outstand aluminium alloy plates in compression, respectively, where the ratios of $N_{u,FE}(M_{u,FE})/N_{fi,AA,Rd}(M_{fi,AA,Rd})$ are plotted against the plate slenderness $\bar{\lambda}_p$. In comparison to EN 1999-1-2 [23] and T/CECS 756-2020 [24], AA 2015 [25] yields more accurate and consistent resistance predictions for aluminium alloy plates, mainly due to the rational use of the elevated- temperature material properties in the design. However, it can be seen from Table 7 that AA 2015 predictions still remain conservative and scattered for both compressive and bending resistances of aluminium alloy plates in fire, with scope for improvements in terms of accuracy and consistency.

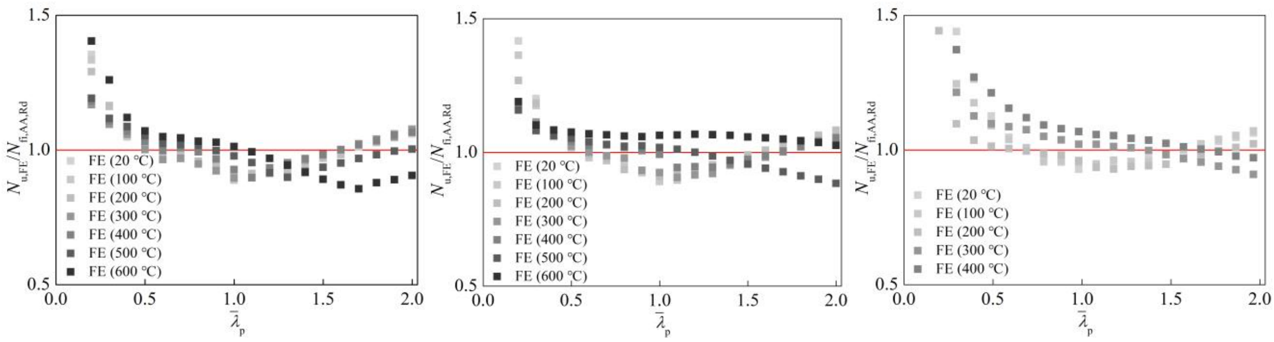

(a) 6061-T6 (b) 6063-T5 (c) 7A04-T6

Fig. 12. Comparisons between FE results and resistance predictions according to AA 2015 [25] for internal plates in compression at different elevated temperatures

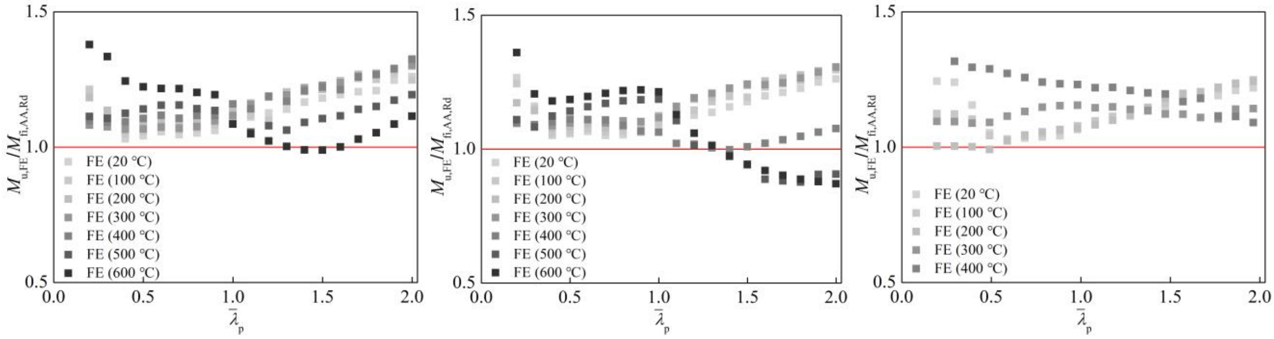

(a) 6061-T6 (b) 6063-T5 (c) 7A04-T6

Fig. 13. Comparisons between FE results and resistance predictions according to AA 2015 [25] for internal plates in bending at different elevated temperatures

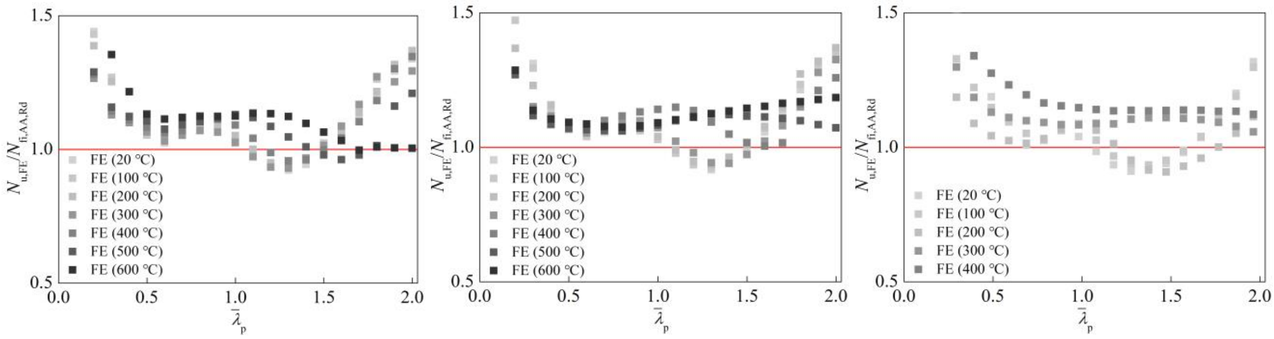

(a) 6061-T6 (b) 6063-T5 (c) 7A04-T6

Fig. 14. Comparisons between FE results and resistance predictions according to AA 2015 [25] for outstand plates in compression at different elevated temperatures

3.3 Continuous Strength Method (CSM)

The CSM is a deformation-based design approach which was firstly proposed for determining the local buckling resistances of stainless steel elements [43], while the approach has recently been extended to cover the design of aluminium alloy structural elements [26] and structures in fire [16]. The CSM enables a continuous, rational and accurate allowance of material nonlinearity (i.e. the spread of plasticity and strain hardening). The applicability and accuracy of the CSM for aluminium alloy plates in fire has been assessed in this subsection.

Central to the CSM is the employment of a base curve to determine the maximum strain that a plate can endure prior to local buckling, as expressed in Eq. (6),

$$\frac{\varepsilon_{\mathrm{csm},\theta}}{\varepsilon_{\mathrm{y},\theta}}=\begin{cases}\dfrac{0.25}{\bar{\lambda}_{\mathrm{p},\theta}^{3.6}}\ \text{but}\ \dfrac{\varepsilon_{\mathrm{csm},\theta}}{\varepsilon_{\mathrm{y},\theta}}\le\min\left(15,\dfrac{C_{1,\mathrm{csm}}\varepsilon_{\mathrm{u},\theta}}{\varepsilon_{\mathrm{y},\theta}}\right) & \text{For}\ \bar{\lambda}_{\mathrm{p},\theta}\le 0.68\\ \dfrac{1}{\bar{\lambda}_{\mathrm{p},\theta}^{1.05}}-\dfrac{0.222}{\bar{\lambda}_{\mathrm{p},\theta}^{2.1}} & \text{For}\ \bar{\lambda}_{\mathrm{p},\theta}>0.68\end{cases}\tag{6}$$

where $\varepsilon_{\mathrm{csm},\theta}$ is the maximum strain that a plate can resist prior to failure at temperature θ, $\varepsilon_{\mathrm{y},\theta}$ is the yield strain at temperature θ that equals to $f_{0.2,\theta}/E_\theta$, $\varepsilon_{\mathrm{u},\theta}$ is the ultimate strain at temperature θ, and $C_{1,\mathrm{csm}} = 0.5$ is a coefficient corresponding to the adopted CSM bilinear material model for aluminium alloys [26]. The CSM resistances can then be calculated utilising the limiting strain $\varepsilon_{\mathrm{csm},\theta}$ determined from the CSM base curve (Eq. (6)), in conjunction with the CSM bilinear material model. The CSM resistance functions for plates in compression ($N_{\mathrm{fi,csm,Rd}}$) and bending ($M_{\mathrm{fi,csm,Rd}}$) are given by Eqs. (7) and (8) [44,45], respectively,

$$N_{\mathrm{fi,csm,Rd}}=\begin{cases}\left(f_{0.2,\theta}+E_{\mathrm{sh},\theta}\varepsilon_{\mathrm{y},\theta}\left(\dfrac{\varepsilon_{\mathrm{csm},\theta}}{\varepsilon_{\mathrm{y},\theta}}-1\right)\right)A & \text{For}\ \bar{\lambda}_{\mathrm{p},\theta}\le 0.68\\ \dfrac{\varepsilon_{\mathrm{csm},\theta}}{\varepsilon_{\mathrm{y},\theta}}f_{0.2,\theta}A & \text{For}\ \bar{\lambda}_{\mathrm{p},\theta}>0.68\end{cases}\tag{7}$$

$$M_{\mathrm{fi,csm,Rd}}=\begin{cases}\left(1+\dfrac{E_{\mathrm{sh},\theta}}{E_\theta}\dfrac{W_{\mathrm{el}}}{W_{\mathrm{pl}}}\left(\dfrac{\varepsilon_{\mathrm{csm},\theta}}{\varepsilon_{\mathrm{y},\theta}}-1\right)-\left(1-\dfrac{W_{\mathrm{el}}}{W_{\mathrm{pl}}}\right)\bigg/\left(\dfrac{\varepsilon_{\mathrm{csm},\theta}}{\varepsilon_{\mathrm{y},\theta}}\right)^{\alpha}\right)W_{\mathrm{pl}}f_{0.2,\theta} & \text{For}\ \bar{\lambda}_{\mathrm{p},\theta}\le 0.68\\ \dfrac{\varepsilon_{\mathrm{csm},\theta}}{\varepsilon_{\mathrm{y},\theta}}W_{\mathrm{el}}f_{0.2,\theta} & \text{For}\ \bar{\lambda}_{\mathrm{p},\theta}>0.68\end{cases}\tag{8}$$

where $E_{\mathrm{sh},\theta}$ is the strain hardening slope and α is the dimensionless coefficient [45].

Comparisons between the CSM resistance predictions and the FE results are shown in Figs. 15-17 for internal aluminium alloy plates in pure compression and pure bending and outstand aluminium alloy plates in compression, respectively. It can be seen from Figs. 15-17 that the degree of conservatism of the CSM predictions for stocky plates (i.e. $\bar{\lambda}_{\mathrm{p},\theta} \le 0.68$) is reduced compared with the three codified design methods due to the consideration of the strain-hardening of the material. However, there is still a fair proportion of the predicted results for the internal plates in compression at high temperatures lying on the unsafe side.

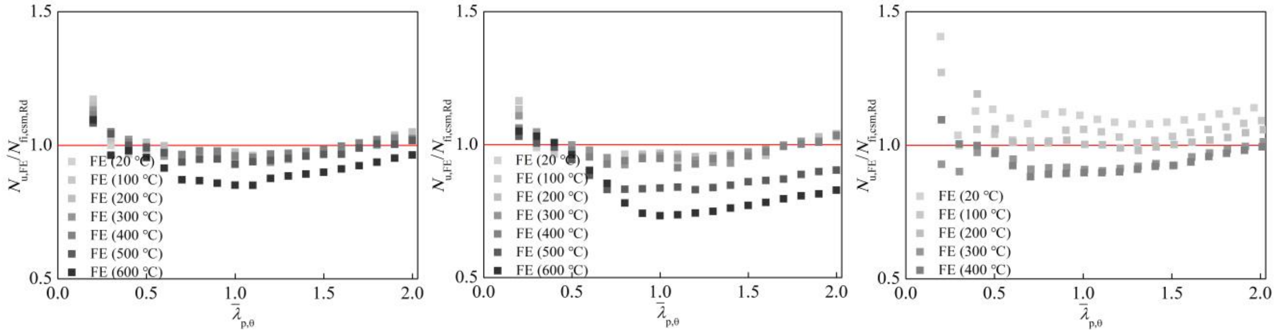

(a) 6061-T6 (b) 6063-T5 (c) 7A04-T6

Fig. 15. Comparisons between FE results and resistance predictions according to CSM [26] for internal plates in compression at different elevated temperatures

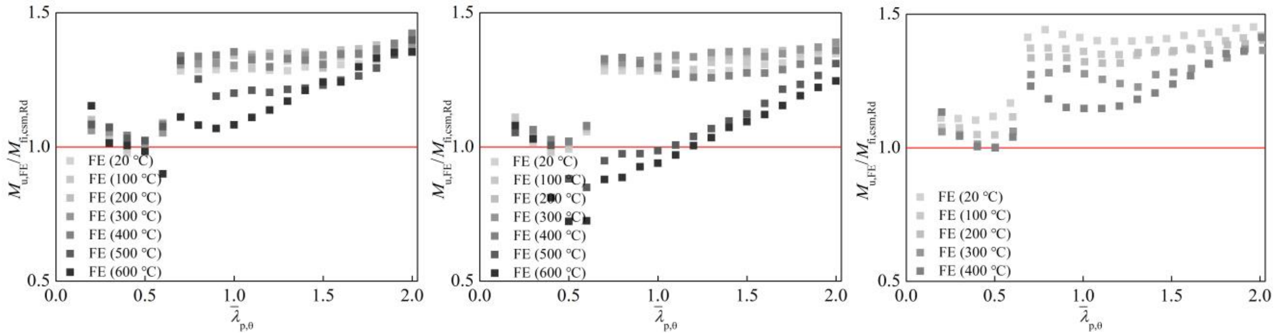

(a) 6061-T6 (b) 6063-T5 (c) 7A04-T6

Fig. 16. Comparisons between FE results and resistance predictions according to CSM [26] for internal plates in bending at different elevated temperatures

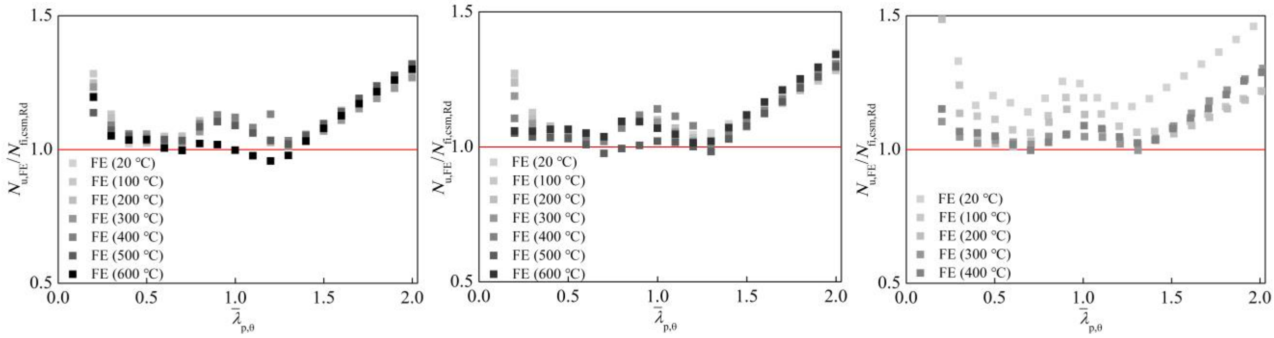

(a) 6061-T6 (b) 6063-T5 (c) 7A04-T6

Fig. 17. Comparisons between FE results and resistance predictions according to CSM [26] for outstand plates in compression at different elevated temperatures

3.4 Design proposals by Maljaars et al. [21] and van der Meulen [22]

Maljaars et al. [21] and van der Meulen [22] proposed new design methods for calculating the resistances of aluminium alloy plates in fire, aiming at improving the accuracy of the current codified approaches. These two proposals are also assessed in this subsection.

3.4.1 Design proposals by Maljaars et al. [21] for aluminium alloy plates in compression

Maljaars et al. [19-21] conducted fire tests on 5083-H111 and 6060-T66 aluminium alloy stub columns and proposed a new equation for determining the effective thickness ratio ρ_c, as given by Eq. (9),

$$\rho_{c,Mal} = \begin{cases} \dfrac{1}{\overline{\lambda}_{p,in,\theta}} + 0.2\dfrac{1}{\overline{\lambda}_{p,in,\theta}^{2}} - 2.5\dfrac{1}{\overline{\lambda}_{p,in,\theta}^{3}} + 2.3\dfrac{1}{\overline{\lambda}_{p,in,\theta}^{4}} \leq 1.0 & (\text{For internal plates}) \\ \dfrac{1}{\overline{\lambda}_{p,in,\theta}} + 1.5\dfrac{1}{\overline{\lambda}_{p,in,\theta}^{2}} - 5\dfrac{1}{\overline{\lambda}_{p,in,\theta}^{3}} + 3.5\dfrac{1}{\overline{\lambda}_{p,in,\theta}^{4}} \leq 1.0 & (\text{For outstand plates}) \end{cases} \tag{9}$$

where $\overline{\lambda}_{p,in,\theta} = (f_{0.2,\theta}/\sigma_{cr,in,\theta})^{0.5}$, in which $\sigma_{cr,in,\theta}$ is the inelastic critical buckling stress at temperature θ that can be determined according to the formulae provided in [21]. Note that $\sigma_{cr,in,\theta}$ in place of $\sigma_{cr,\theta}$ was used in Maljaars's proposal [21] to consider the effects of the nonlinear behaviour of the aluminium alloy below $f_{0.2,\theta}$ on the buckling behaviour of plates in fire. Following this, the resistance of an aluminium alloy plate in compression can be calculated as $N_{fi,Mal,Rd} = \rho_{c,Mal}Af_{0.2,\theta}$.

Comparisons between predictions determined by using Maljaars's method [21] and FE results are shown in Figs. 18 and 19. It can be observed from the figures that the design proposal by Maljaars et al. [21] provides more accurate and less scattered resistance predictions compared to the current design methods in European, Chinese and American codes. However, the predicted results for internal plates are unconservative in some cases, especially for those at elevated temperatures equal to or greater than 500 °C; this might be explained due to the fact that the parameters used in Eq. (9) were proposed underpinned by experimental results on 5083-H111 and 6060-T66 aluminium alloy stub columns, while the suitability of these parameters in Eq. (9) for aluminium plates made of other aluminium alloy grades requires further research. It should be noted that there is an increase in the calculation effort for using Maljaars's method [21] as the inelastic critical buckling stress at temperature θ ($\sigma_{cr,in,\theta}$) should be determined by solving implicit equations by means of iteration. Hence there is still a clear need for a safer and simpler approach for the design of fire resistances of aluminium alloy plates in compression.

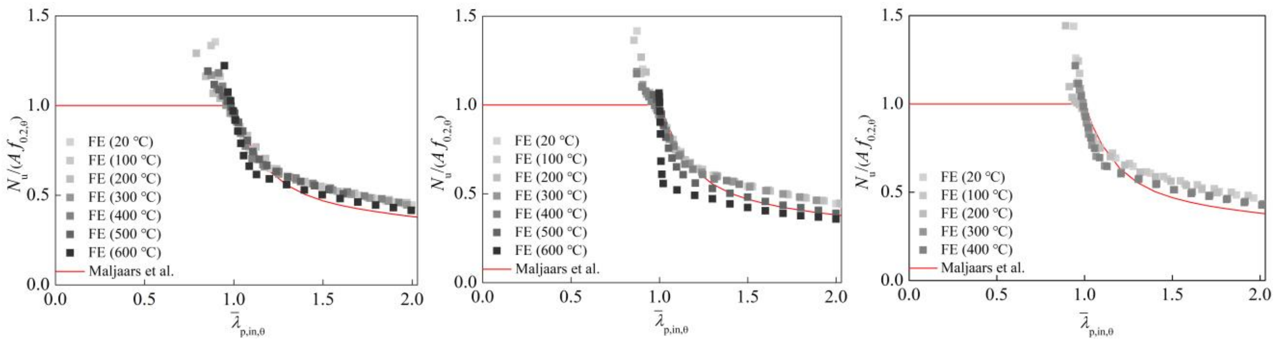

(a) 6061-T6 (b) 6063-T5 (c) 7A04-T6

Fig. 18. Comparisons between FE results and resistance predictions according to Maljaars et al. [21] for internal plates in compression at different elevated temperatures

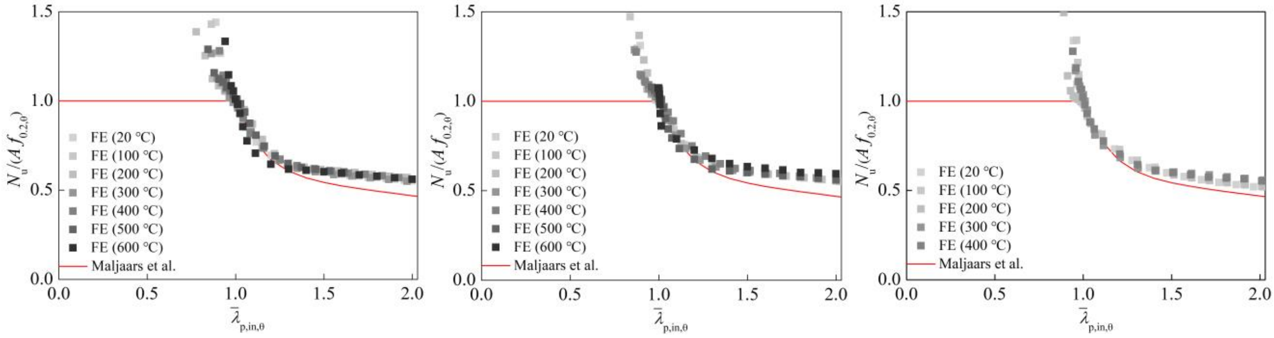

(a) 6061-T6 (b) 6063-T5 (c) 7A04-T6

Fig. 19. Comparisons between FE results and resistance predictions according to Maljaars et al. [21] for outstand plates in compression at different elevated temperatures

3.4.2 Design proposals by van der Meulen [22] for aluminium alloy plates in bending

van der Meulen [22] proposed a new design method for aluminium alloy plates in bending under fire conditions on the basis of the design approach set out in EN 1999-1-2 [23]. For Class 4 plates, a new equation for determining the effective thickness ratio ρ_c was proposed, as given by Eq. (10), where a temperature-related material factor ε_θ was used in replace of ε in Eq. (6.12) of EN 1999-1-2 [23].

$$\rho_{c,van} = \frac{C_{1,van}}{(\beta/\varepsilon_\theta)} - \frac{C_{2,van}}{(\beta/\varepsilon_\theta)^2} \le 1.0 \tag{10}$$

In Eq. (10), $C_{1,van}$ and $C_{2,van}$ are proposed constants and ε_θ is the temperature-related material factor given by Eq. (11).

$$\varepsilon_\theta = (250E_\theta/f_{0.2,\theta}/E)^{0.5} \tag{11}$$

The fire resistances of aluminium alloy plates in bending can be determined by Eq. (12),

$$M_{fi,van,Rd} = \alpha_{Mi} W_{el} f_{Mi,\theta} \quad (i=1,2,3,4) \tag{12}$$

where α_{Mi} is the shape factor defined in Section 6.2.5 of EN 1999-1-2 [23] and $f_{Mi,\theta}$ represents the stress at a specified strain. For Class 1 plates, $f_{M1,\theta}$ is equal to the stress corresponding to $2\varepsilon_{0.2,\theta}$; for Class 2 plates, $f_{M2,\theta}$ should be determined in accordance with the width to thickness ratio of the plate, the details of which are described in Section 5.5.5 of [22]; for Class 3 and Class 4 plates, $f_{M3,\theta}$ and $f_{M4,\theta}$ are all equal to the yield strength $f_{0.2,\theta}$.

Comparisons between the predictions determined by using van der Meulen's proposal ($M_{fi,van,Rd}$) and numerical results are illustrated in Fig. 20 and summarised in Table 7. As can be seen from Fig. 20, the fire resistances predicted by the new proposal for stocky plates in bending are reasonable due to replacing $f_{0.2,\theta}$ with $f_{M1,\theta}$ or $f_{M2,\theta}$, which takes due consideration of the strain-hardening of aluminium alloys in fire. With regards to slender cross sections, resistances derived from this proposal are more accurate than those predicted by European and Chinese codes while it should be noted that the safety margin of $M_{fi,van,Rd}$ decreases with increasing temperatures and even falls into the unsafe side, which is opposite to the tendency of the resistance predictions by EN 1999-1-2 [23] and T/CECS 756-2020 [24] as shown in Figs. 7 and 10. This might be resulted from the neglect of the higher degree of roundedness of the stress-strain curves with increasing temperature, which leads to less conservative or even unsafe resistance predictions for aluminium alloy plates at greater elevated temperatures. Note that the European and Chinese codes neglect both the variations of $k_{0,\theta}/k_{E,\theta}$ and the degree of the roundedness of stress-strain curves at elevated temperatures, though the effect of the former predominates.

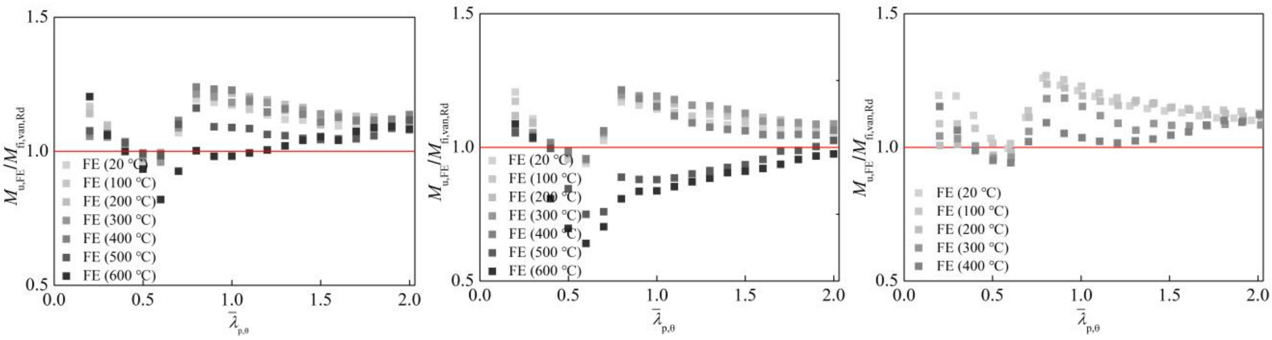

(a) 6061-T6 (b) 6063-T5 (c) 7A04-T6

Fig. 20. Comparisons between FE results and resistance predictions according to van der Meulen [22] for internal plates in bending at different elevated temperatures

Table 7 Comparisons of numerical results with resistance predictions using different methods for aluminium alloy plates at different elevated temperatures

Design method	Plate type	Loading condition	$N(M)_{u,FE} / N(M)_{fi,pred,Rd}$ (at different temperatures)						
			20 °C	100	200	300	400	500	600

				°C	°C	°C	°C	°C	°C	°C
EN 1999-1-2 [23]	Internal plates	Compression	Mean	1.05	1.04	1.04	1.13	1.20	1.23	1.36
			COV	0.153	0.121	0.084	0.193	0.208	0.182	0.247
	Internal plates	Bending	Mean	1.17	1.17	1.20	1.33	1.42	1.39	1.52
			COV	0.088	0.090	0.094	0.217	0.216	0.177	0.175
	Outstand plates	Compression	Mean	1.20	1.19	1.20	1.30	1.38	1.43	1.55
			COV	0.140	0.114	0.093	0.199	0.206	0.232	0.267
T/CECS 756-2020 [24]	Internal plates	Compression	Mean	1.07	1.05	1.06	1.15	1.23	1.26	1.40
			COV	0.146	0.115	0.080	0.191	0.206	0.199	0.263
	Internal plates	Bending	Mean	1.31	1.32	1.34	1.48	1.57	1.55	1.69
			COV	0.170	0.154	0.118	0.180	0.193	0.137	0.140
	Outstand plates	Compression	Mean	1.20	1.19	1.20	1.30	1.39	1.43	1.55
			COV	0.138	0.113	0.093	0.204	0.209	0.229	0.265
AA 2015 [25]	Internal plates	Compression	Mean	1.03	1.03	1.01	1.02	1.06	1.00	1.04
			COV	0.163	0.127	0.097	0.125	0.168	0.070	0.101
	Internal plates	Bending	Mean	1.13	1.15	1.15	1.15	1.16	1.08	1.10
			COV	0.065	0.066	0.075	0.061	0.091	0.087	0.124
	Outstand plates	Compression	Mean	1.13	1.12	1.10	1.12	1.16	1.10	1.13
			COV	0.162	0.155	0.136	0.117	0.147	0.060	0.085
CSM [26]	Internal plates	Compression	Mean	1.03	1.01	1.03	0.97	0.97	0.93	0.88
			COV	0.082	0.060	0.158	0.048	0.051	0.075	0.108
	Internal plates	Bending	Mean	1.27	1.26	1.36	1.25	1.23	1.13	1.08
			COV	0.109	0.106	0.185	0.104	0.101	0.119	0.148
	Outstand plates	Compression	Mean	1.17	1.13	1.11	1.10	1.11	1.09	1.09
			COV	0.128	0.097	0.083	0.076	0.074	0.086	0.091
Maljaars et al. [21]	Internal plates	Compression	Mean	1.12	1.11	1.09	1.06	1.06	1.01	0.90
			COV	0.149	0.120	0.101	0.092	0.092	0.084	0.184
	Outstand plates	Compression	Mean	1.13	1.13	1.14	1.12	1.13	1.08	1.09
			COV	0.160	0.154	0.146	0.145	0.142	0.061	0.095
van der Meulen [22]	Internal plates	Bending	Mean	1.11	1.12	1.11	1.10	1.08	1.00	0.95
			COV	0.064	0.063	0.065	0.065	0.064	0.097	0.129
New proposals	Internal plates	Compression	Mean	1.07	1.06	1.05	1.05	1.08	1.05	1.05
			COV	0.143	0.103	0.069	0.072	0.067	0.033	0.047
	Internal plates	Bending	Mean	1.08	1.09	1.09	1.12	1.13	1.06	1.07
			COV	0.062	0.051	0.052	0.070	0.063	0.051	0.080
	Outstand plates	Compression	Mean	1.12	1.11	1.10	1.12	1.16	1.13	1.20
			COV	0.165	0.140	0.102	0.107	0.101	0.071	0.101

4. New proposals

As discussed in the previous section, there is a clear need for a simple yet more accurate and consistent design method for the local buckling resistances of aluminium alloy plates in fire. Towards meeting this need, a simplified cross-section classification approach is first proposed in this section. Following this, new design formulae on the basis of the effective thickness method are derived and discussed. Finally, the structural fire performance data obtained from the numerical analyses carried out in the present paper and tests conducted in [19] are utilised to assess the accuracy of the new proposals.

4.1 New cross-section classifications

A simplified approach for classifying aluminium alloy cross sections in fire is proposed in this subsection.

In the new proposals, aluminium alloy plates are categorised into three classes (i.e. stocky, non-stocky and slender) instead of the conventional four classes (i.e. Class 1-4) as specified in EN 1999-1-1 [42].The cross-section classification of an aluminium alloy plate in fire is quantified by the plate slenderness at temperature θ ($\overline{\lambda}_{\mathrm{p},\theta}$). The slenderness limits, i.e. the threshold value between slender and non-stocky cross sections ($\overline{\lambda}_{\mathrm{p0},\theta}$) and the limit between the non-stocky and stocky cross sections ($\overline{\lambda}_{\mathrm{p1},\theta}$), are summarised in Table 8, where a, b and c are constants which are further explained in the following subsection, k is the elastic buckling coefficient, γ_θ equals to $(k_{0,\theta}/k_{\mathrm{E},\theta})^{0.15}$ and η and ψ are stress gradient factors detailed in Section 6.1 of EN 1999-1-1 [42]. Note that Class A and B represent different material buckling classes in accordance with EN 1999-1-1 [42]; in this study, 6061-T6 and 7A04-T6 alloys belong to Class A, while 6063-T5 belongs to Class B.

Table 8 Summary of key parameters in new proposals

Plate type	Material classification	a	b	c	$\overline{\lambda}_{\mathrm{p0},\theta}$	$\overline{\lambda}_{\mathrm{p1},\theta}$
Internal plate	Class A	0.970	1.000	0.058	$(0.485+(0.235-0.058(3+\psi))^{0.5})\gamma_\theta$	$\gamma_\theta\,(1.012/k\eta^2)^{0.5}$
	Class B	0.990	1.000	0.058	$(0.495+(0.245-0.058(3+\psi))^{0.5})\gamma_\theta$	$\gamma_\theta(1.076/k\eta^2)^{0.5}$
Outstand plate	Class A	0.780	0.750	0.013	$0.697\gamma_\theta$	$\gamma_\theta(0.08/k)^{0.5}$
	Class B	0.870	0.750	0.013	$0.811\gamma_\theta$	$\gamma_\theta(0.08/k)^{0.5}$

4.2 New effective thickness method

A new effective thickness method, using a similar format as that provided in EN 1993-1-5 [11], is proposed in this subsection for aluminium alloy plates in fire. The new proposal takes into account the different loading and boundary conditions as well as features of the aluminium alloy material properties in fire: (1) the different deterioration rates of $f_{0.2,\theta}$ and E_θ, and (2) the different levels of the roundness of the stress-strain curves below $f_{0.2,\theta}$, as given by Eqs. (13) and (14) for internal ($\rho_{\mathrm{c,int}}$) and outstand ($\rho_{\mathrm{c,out}}$) plates, respectively,

$$\rho_{\mathrm{c,int}}=\begin{cases}1 & \overline{\lambda}_{\mathrm{p},\theta}\le\overline{\lambda}_{\mathrm{p0},\theta}\\ \dfrac{a}{(\overline{\lambda}_{\mathrm{p},\theta}/\gamma_\theta)^{b}}-\dfrac{c(3+\psi)}{(\overline{\lambda}_{\mathrm{p},\theta}/\gamma_\theta)^{2b}} & \overline{\lambda}_{\mathrm{p},\theta}>\overline{\lambda}_{\mathrm{p0},\theta}\end{cases}\tag{13}$$

$$\rho_{\mathrm{c,out}}=\begin{cases}1 & \overline{\lambda}_{\mathrm{p},\theta}\le\overline{\lambda}_{\mathrm{p0},\theta}\\ \dfrac{a}{(\overline{\lambda}_{\mathrm{p},\theta}/\gamma_\theta)^{b}}-\dfrac{c}{(\overline{\lambda}_{\mathrm{p},\theta}/\gamma_\theta)^{2b}} & \overline{\lambda}_{\mathrm{p},\theta}>\overline{\lambda}_{\mathrm{p0},\theta}\end{cases}\tag{14}$$

where a, b and c are constants obtained by regression analysis and summarised in Table 8.

The proposed equations for determining the compressive and bending resistances of aluminium alloy plates in fire are summarised in Table 9, where the effective cross-section properties (A_{eff} and W_{eff}) should be calculated using the proposed effective thickness method as described above. For aluminium alloy plates in compression, it is recommended to use the gross area of the cross section (A) for stocky and non-stocky plates in fire and the effective cross-section aera (A_{eff}) for slender plates in fire. With regards to aluminium alloy plates in bending, the plastic (W_{pl}), elastic (W_{el}) and effective (W_{eff}) cross-section modulus are respectively used for stocky, non-stocky and slender plates at elevated temperatures. Besides, a parameter $\alpha_{\mathrm{u},\theta}$ is proposed to allow a linear transition between $M_{\mathrm{pl},\theta}$ (= $W_{\mathrm{pl}}f_{0.2}k_{0,\theta}$) and $M_{\mathrm{el},\theta}$ (= $W_{\mathrm{el}}f_{0.2}k_{0,\theta}$) for non-stocky plates in bending, as given by Eq. (15),

$$\alpha_{\mathrm{u},\theta} = 1 + \left(\left(\bar{\lambda}_{\mathrm{p0},\theta} - \bar{\lambda}_{\mathrm{p},\theta}\right) / \left(\bar{\lambda}_{\mathrm{p0},\theta} - \bar{\lambda}_{\mathrm{p1},\theta}\right)\right)\left(W_{\mathrm{pl}} / W_{\mathrm{el}} - 1\right) \tag{15}$$

Table 9 Proposed equations for determining compressive and bending resistances of aluminium alloy plates in fire

Cross-section classification	Load condition	
	Compression	Bending
Stocky	$Af_{0.2}k_{0,\theta}$	$W_{\mathrm{pl}}f_{0.2}k_{0,\theta}$
Non-stocky	$Af_{0.2}k_{0,\theta}$	$\alpha_{\mathrm{u},\theta}W_{\mathrm{el}}f_{0.2}k_{0,\theta}$
Slender	$A_{\mathrm{eff}}f_{0.2}k_{0,\theta}$	$W_{\mathrm{eff}}f_{0.2}k_{0,\theta}$

4.3 Assessment of new design proposals

The accuracy of the resistance predictions of aluminium alloy plates in fire determined from the new design proposals was assessed in this subsection, where numerical data are compared with the resistance predictions in Figs. 21-23 for internal aluminium alloy plates in pure compression and pure bending and outstand aluminium alloy plates in compression, respectively. Different design buckling curves for aluminium alloy plates at varying elevated temperatures according to Eqs. (13) and (14) are also plotted in Figs. 21-23 for comparison purposes. The comparisons reveal that the new proposals can predict the compressive and bending resistances of aluminium alloy plates in fire with substantially improved accuracy and consistency. Moreover, the proposed method provides continuous resistance predictions for aluminium alloy plates with varying slendernesses in bending thus avoiding any discontinuity in resistance predictions in current codified methods (i.e. a step from $M_{\mathrm{pl},\theta}$ (= $W_{\mathrm{pl}}f_{0.2}k_{0,\theta}$) and $M_{\mathrm{el},\theta}$ (= $W_{\mathrm{el}}f_{0.2}k_{0,\theta}$) at the border between Class 2 and Class 3 plates in EN 1999-1-2 [23]). The comparison results, including the test data collected from the literature (6060-T66 stub columns by Maljaars et al. [19]) and FE data for all the investigated aluminium alloy plates, are shown in Fig. 24, confirming the excellent accuracy and consistency of the proposed method.

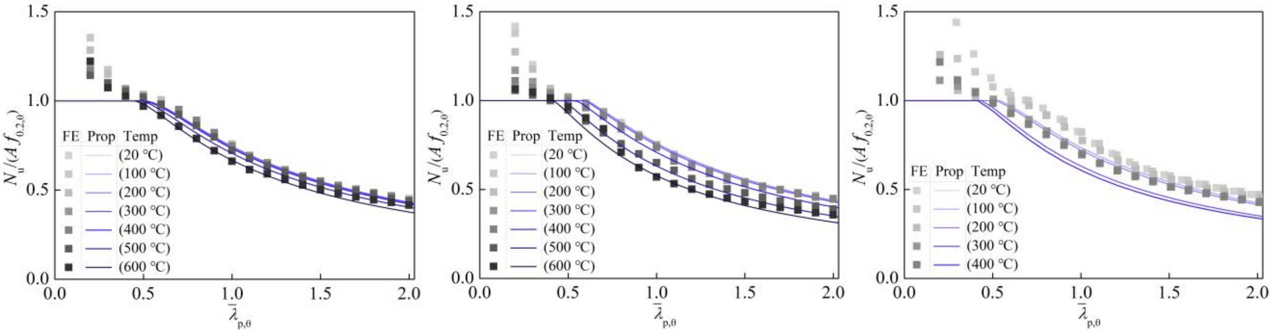

(a) 6061-T6 (b) 6063-T5 (c) 7A04-T6

Fig. 21. Comparisons between FE results and resistance predictions according to the proposed method for internal plates in compression at different elevated temperatures

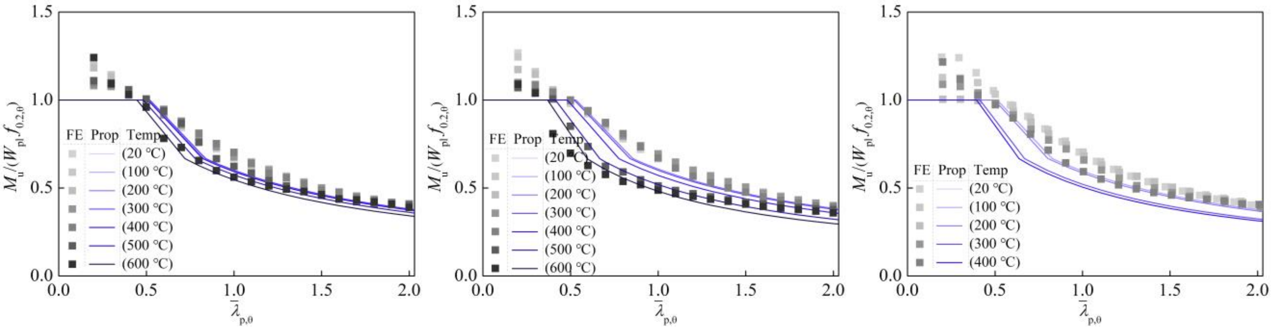

(a) 6061-T6 (b) 6063-T5 (c) 7A04-T6

Fig. 22. Comparisons between FE results and resistance predictions according to the proposed method for internal plates in bending at different elevated temperatures

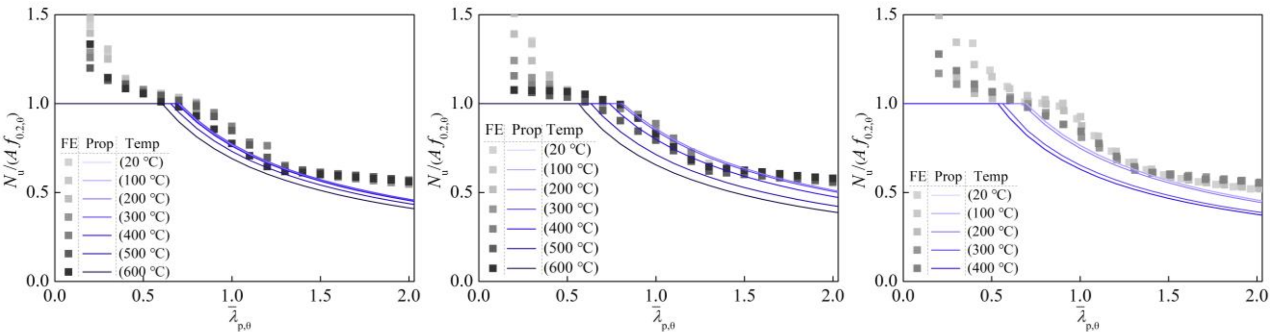

(a) 6061-T6 (b) 6063-T5 (c) 7A04-T6

Fig. 23. Comparisons between FE results and resistance predictions according to the proposed method for outstand plates in compression at different elevated temperatures

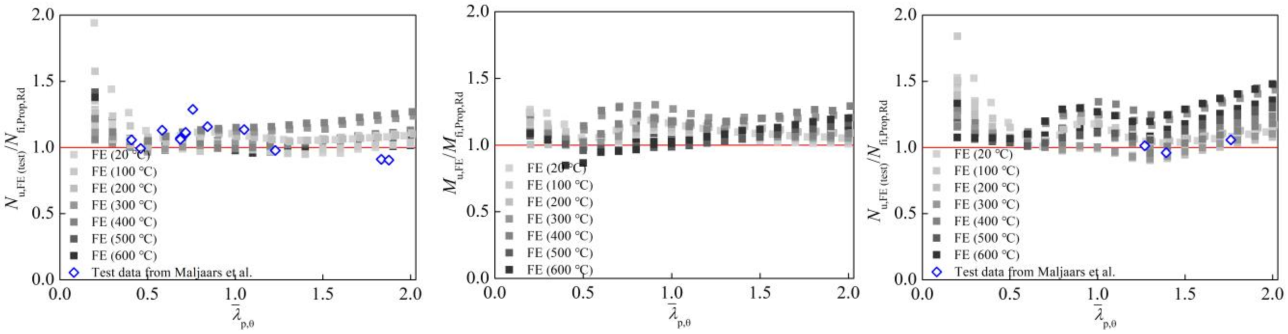

(a) Internal plates in compression (b) Internal plates in bending (c) Outstand plates in compression

Fig. 24. Summary of the comparisons between FE/test results and resistance predictions according to the proposed method at different elevated temperatures

5. Reliability assessment

The reliability of the new proposals as well as the other design methods is assessed in this section according to the three reliability criteria proposed by Kruppa [27], which have been widely utilised to assess the reliability of fire design methods for metallic structures [12,13]. These criteria assess the level of overestimation by the design method and control the structural risk under fire conditions, as described below:

- Criterion 1: the predicted resistances by the design method should not be greater than 115% of the experimentally or numerically obtained resistances, i.e. $N_{fi,pred,Rd} \leq 1.15\ N_{u,FE(tests)}$;
- Criterion 2: the number of the unsafe predictions should be less than 20% of the total number of predictions, i.e. number ($N_{fi,pred,Rd} > N_{u,FE(tests)}$) / number ($N_{fi,pred,Rd}$) ≤ 20%;
- Criterion 3: The mean value of percentage differences between the predicted resistances and experimental or numerical resistances should be less than zero, i.e. $\overline{X}\ [(N_{fi,pred,Rd}-N_{u,FE(tests)})/N_{u,FE(tests)}] \leq 0$.

The design method may be deemed reliable should the predicted resistances by the design method satisfy the three reliability criteria, and vice versa. The assessment results are summarised in Table 10, where the values listed in the 3rd to 5th columns represent the percentage of the resistance predictions on the unsafe side by more than 15% of the experimental or FE resistances (Criterion 1), the percentage of resistance predictions on the unsafe side of the experimental or numerical resistances (Criterion 2), and the average value of all percentage differences between the resistance predictions and the experimental or numerical resistances (Criterion 3), respectively. The results that fail to satisfy the criteria are marked with a "*". As can be seen from Table 10, the new proposals satisfy all the three criteria, though for plates in bending the criterion 1 is marginally violated. The European [23] and Chinese codes [24] satisfy the three criteria but their predictions are unduly conservative with the values for Criterion 3 being less than -20%. The American code [25] and the CSM [26] violate the Criteria 1 and 2, and the proposals by Maljaars et al. [21] and van der Meulen [22] also exhibit a lower level of reliability than the design method proposed in the present study. In conclusion, the new proposals are sufficiently reliable and can provide safe predictions for the design of aluminium alloy plates in fire.

Table 10 Reliability assessment of different design methods for aluminium alloy plates in fire

Design method	Loading condition	Criterion 1 (%)	Criterion 2 (%)	Criterion 3 (%)
New proposal	Compression	0.00	14.68	-9.56
	Bending	0.55*	6.93	-9.46
EN 1999-1-2 [23]	Compression	0.00	11.63	-21.93
	Bending	0.00	1.94	-29.93
T/CECS 756-2020 [24]	Compression	0.00	8.86	-23.17
	Bending	0.00	0.00	-44.97
AA ADM [25]	Compression	0.14*	31.72*	-7.27
	Bending	0.00	4.99	-13.68
CSM [26]	Compression	3.88*	35.32*	-4.92
	Bending	1.11*	6.37	-23.84
Maljaars et al. [21]	Compression	2.77*	21.19*	-8.94
van der Meulen [22]	Bending	3.32*	19.94	-7.49

6. Conclusions

A comprehensive numerical investigation into the structural performance of aluminium alloy plates in fire has been conducted in the present study. FE models were established and validated against the experimental results collected from the literature. Based upon the validated models, a series of parametric studies, covering a wide range of aluminium alloy grades, plate slendernesses, temperature levels as well as loading and boundary conditions, has been conducted. The generated numerical results were then utilised to evaluate the accuracy and reliability of existing design methods for fire resistances of aluminium alloy plates. New design proposals were finally proposed underpinned by the numerical database. It has been found that the new design proposals are able to provide more accurate, consistent and reliable resistance predictions for aluminium alloys plates in fire than the existing design approaches. The main conclusions drawn from the present study are summarised as follows:

1. FE models that consider both the thermal expansion and the geometric and material nonlinearities were established in the present study. The developed FE models were shown to be capable of accurately replicating the structural performance of aluminium alloy elements in fire, including the failure modes, load-carrying capacities and load-displacement histories.
2. The European and Chinese codes yield rather conservative resistance predictions of aluminium alloy

plates in fire, especially for those at higher (> 300 °C) elevated temperatures. The design approaches specified in the American code and the CSM [26], which employ the elevated-temperature material properties for the calculation of the fire resistances of aluminium alloy plates, result in more accurate resistance predictions but fail to satisfy the three safety criteria [27]. The recently developed methods by Maljaars et al. [21] and van der Meulen [22] can provide resistance predictions with improved accuracy but lead to a significant number of data points lying on the unsafe side for plates at temperatures higher than 400 °C; these methods are also shown to frequently violate the three reliability criteria [27], especially for aluminium alloy plates at higher elevated temperatures.

3. The new design proposals, developed based on the comprehensive numerical analyses presented in this study, have been shown to provide more accurate, consistent and reliable resistance predictions for aluminium alloy plates in fire than the existing design approaches.

Acknowledgements

The authors would like to acknowledge the financial support provided by the National Natural Science Foundation of China (Grant No. 52108165).

References

[1] Mazzolani FM. Aluminium alloy structures. Second edition. E & FN Spon. London; 1995.

[2] Wang YQ, Wang ZX, Yin FX, Yang L, Shi YJ, Yin J. Experimental study and finite element analysis on the local buckling behavior of aluminium alloy beams under concentrated loads. Thin-Walled Structures. 2016;105:44-56.

[3] Su MN, Young B, Gardner L. Testing and design of aluminum alloy cross sections in compression. Journal of Structural Engineering. 2014;140(9):04014047.

[4] Wang ZX, Li MY, Han QH, Yun X, Zhou K, Gardner L, Mazzolani FM. Structural fire behaviour of aluminium alloy structures: Review and outlook. Engineering Structures. 2022;268:114746.

[5] Wang ZX, Ma CY, Li MY, Han QH, Li HT, Zhao DD. Mechanical properties of 7A04-T6 high strength structural aluminium alloy at elevated temperatures and after cooling down. Thin-Walled Structures. 2022;180:109930.

[6] Su MN and Young B. Material properties of normal and high strength aluminium alloys at elevated temperatures. Thin-Walled Structures. 2019;137:463-471.

[7] Toric N, Brnic J, Boko I, Brcic M, Burgess IW, Uzelac I. Experimental analysis of the behaviour of aluminium alloy EN 6082AW T6 at high temperature. Metals. 2017;7(4):126.

[8] Kaufman JG. Properties of aluminum alloys: Tensile, creep, and fatigue data at high and low temperatures. Washington D.C.: ASM International, Material Park; 1999.

[9] EN 1993-1-2, Eurocode 3: Design of steel structures-Part 1-2: General rules-Structural fire design. European Committee for standardization. Brussels; 2005.

[10] Couto C, Real PV, Lopes N, Zhao B. Effective width method to account for the local buckling of steel thin plates at elevated temperatures. Thin-Walled Structures. 2014;84:134-149.

[11] EN 1993-1-5, Eurocode 3: Design of steel structures-Part 1-5: Plated structural elements. European Committee for Standardization. Brussels; 2006.

[12] Xing Z, Kucukler M, Gardner L. Local buckling of stainless steel plates in fire. Thin-Walled Structures. 2020;148:106570.

[13] Kucukler M. Local stability of normal and high strength steel plates at elevated temperatures. Engineering Structures. 2021;243:112528.

[14] Wang WY, Kodur V, Yang XC, Li GQ. Experimental study on local buckling of axially compressed steel stub columns at elevated temperatures. Thin-Walled Structures. 2014;82:33-45.

[15] Wang WY, Li X, Al-azzani H. Experimental study on local buckling of high-strength Q960 steel columns at elevated temperatures. Journal of Constructional Steel Research. 2021;183:106716.

[16] Yun X, Saari N, Gardner L. Behaviour and design of eccentrically loaded hot-rolled steel SHS and RHS stub columns at elevated temperatures. Thin-Walled Structures. 2020;149:106646.

[17] Yang KC, Chen SJ, Lin CC, Lee HH. Experimental study on local buckling of fire-resisting steel columns under fire load. Journal of Constructional Steel Research. 2005;61:553-565.

[18] AISC, Manual of steel construction, load and resistance factor design. AISC Manual Committee. Chicago; 2001.

[19] Maljaars J, Soetens F, Snijder HH. Local buckling of aluminium structures exposed to fire. Part1: Tests. Thin-Walled Structures. 2009;47:1404-1417.

[20] Maljaars J, Soetens F, Snijder HH. Local buckling of aluminium structures exposed to fire. Part 2: Finite element models. Thin-Walled Structures. 2009;47:1418-1428.

[21] Maljaars J, Soetens F, Snijder HH. Local buckling of fire-exposed aluminium members: New design model. Journal of Structural Engineering. 2010;136(1):66-75.

[22] van der Meulen OR. Local buckling of aluminium beams in fire conditions. Ph.D. thesis, Eindhoven University of Technology, Eindhoven. 2015.

[23] EN 1999-1-2, Eurocode 9: Design of aluminium structures-Part 1-2: Structural fire design. European Committee for standardization. Brussels; 2007.

[24] T/CECS 756-2020, Technical specification for fire safety of aluminium alloy structures in buildings. Beijing; 2020. (in Chinese)

[25] Aluminum design manual. The Aluminum Association. Washington D.C.; 2015.

[26] Su MN, Young B, Gardner L. The continuous strength method for the design of aluminium alloy structural elements. Engineering Structures. 2016;122:338-348.

[27] Kruppa J. Eurocodes-Fire parts: proposal for a methodology to check the accuracy of assessment methods. CEN TC 250, Horizontal Group Fire, Document no: 99/130; 1999.

[28] ABAQUS. Reference manual, version 6.17. Simulia, Dassault systems. France; 2017.

[29] Yun X, Wang ZX, Gardner L. Structural performance and design of hot-rolled steel SHS and RHS under combined axial compression and bending. Structures. 2020;27:1289-1298.

[30] Zhu JH, Li ZQ, Su MN. Numerical investigation and design of aluminium alloy channel section columns at elevated temperatures. Thin-Walled Structures. 2021;159:107225.

[31] Yuan HX, Wang YQ, Chang T, Du XX, Bu YD, Shi YJ. Local buckling and postbuckling strength of extruded aluminium alloy stub columns with slender I-sections. Thin-Walled Structures. 2015;90:140-149.

[32] Zhu JH and Young B. Tests and design of aluminum alloy compression members. Journal of Structural Engineering. 2006;132:1096-1107.

[33] Wang YQ, Yuan HX, Chang T, Du XX, Yu M. Compressive buckling strength of extruded aluminium alloy I-section columns with fixed-pinned end conditions. Thin-Walled Structures. 2017; 119:396-403.

[34] Feng R, Zhu W, Wan HY, Chen AY, Chen Y. Tests of perforated aluminium alloy SHSs and RHSs under axial compression. Thin-Walled Structures. 2018;130:194-212.

[35] Zhu JH and Young B. Experimental investigation of aluminum alloy thin-walled tubular members in combined compression and bending. Journal of Structural Engineering. 2006;132:1955-1966.

[36] Zhang Y, Bu YD, Wang YQ, Ouyang YW. Study of flexural–torsional buckling behaviour of 6061-T6 aluminium alloy unequal-leg angle columns. Thin-Walled Structures. 2021;164:107821.

[37] EN 1090-2, Execution of steel structures and aluminium structures-part 2: Technical requirements for steel structures. European Committee for standardization. Brussels; 2008.

[38] EN 1090-3, Execution of steel structures and aluminium structures-part 3: Technical requirements for aluminium structures. European Committee for standardization. Brussels; 2008.

[39] Yun X, Wang ZX, Gardner L. Full-range stress-strain curves for aluminum alloys. Journal of Structural Engineering. 2021;147(6):04021060.

[40] Long YL, Zeng L, Gardner L, Wadee MA. A new model for calculating the elastic local buckling stress of steel plates in square CFST columns. Thin-Walled Structures. 2022;171: 108756.

[41] Seif M, Schafer BW. Local buckling of structural steel shapes. Journal of Constructional Steel Research. 2010;66:1232-1247.

[42] EN 1999-1-1, Eurocode 9: Design of aluminium structures-Part 1-1: General structural rules. European Committee for Standardization. Brussels; 2007.

[43] Gardner L. A new approach to structural stainless steel design. Ph.D. thesis, Imperial College London, London. 2002.

[44] Liew A. Design of structural steel elements with the Continuous Strength Method. Ph.D. thesis, Imperial College London, London. 2014.

[45] Gardner L, Yun X, Walport F. The Continuous Strength Method– Review and outlook. Engineering Structures. 2022. (under review)